An Improved FCS-MPC Algorithm for Three-Phase Three-Level T-Type Off-Grid Inverters Based on Current Tracking

Jinyu LV, Yinke DOU, and Yu ZHANG

***Abstract*—This paper presents a finite control set model predictive control (FCS-MPC) strategy for three-phase three-level T-type off-grid inverters, with the aim of optimizing current tracking performance. First, the voltage vector function range and the subsector regions are redefined with the integration of the voltage vector synthesis concept, which helps reduce current ripples and thus total harmonic distortions. Then, to promote neutral point potential balance, a time compensation mechanism is introduced, complementing the passive balance through voltage vector synthesis. To address the issue of high computational complexity, a two-step sector determination strategy is proposed. The proposed FCS-MPC is both tested through simulation and experiment. Compared with the conventional approach, the proposed strategy shows superior results in terms of algorithm execution time, neutral potential balance, steady-state performance, and dynamic response.**

***Index Terms*—FCS-MPC, sector optimization, simplified calculation, time compensation, voltage vector synthesis.**

I. Introduction

As the world's total energy consumption steadily increases, renewable energy has developed rapidly, with solar photovoltaics exhibiting clear advantages [1]. Along with the development of transportation electrification, photovoltaics will be deeply integrated with highways, rail transit, airports and seaports, bringing numerous development opportunities [2]−[6]. The off-grid inverter is a device that connects the DC generator to the load or energy storage device, which is essential for the efficient use of energy. Due to fewer switching devices and lower voltage ratings, the traditional two-level inverter cannot be widely applied in high-voltage and high-power systems. Moreover, although its control strategy is simple, the output voltage and current are highly distorted. However, a method for achieving an effect similar to that of a multilevel inverter via the modular structure of three-phase two-level inverters has been described in [7]. In this context, the three-level topology has been extensively employed in these years. This circuit configuration balances the number of levels and the complexity of control, which can achieve better power output quality and is more suitable for high-power occasions [8]−[12]. The T-type topology is an improvement on the NPC topology and flying capacitor topology, which do not contain clamping diodes and flying capacitors. Its advantages are lower cost and high energy conversion efficiency [13]−[14].

Regarding control strategies, the popular ones include proportional-integral-derivative (PID) control, repetitive control, fuzzy control, deadbeat control, etc. [15]−[18]. PID control is one of the most widely adopted control algorithms in photovoltaic control systems because of its simple algorithm, good robustness, and high reliability. However, due to the complexity of the controlled object's structure, obtaining an accurate mathematical model of the system is challenging, making the design of the PID controller parameters difficult. In practical applications, these control parameters can only be determined through time-consuming field trials. When the operating environment of the system changes, the control parameters must be adjusted accordingly. Otherwise, the stability of the controller cannot be fundamentally guaranteed with the adaptability of the system being reduced. To overcome these problems, one promising technique is model predictive control (MPC), which is an optimal control algorithm based on system predictive model, rolling optimization and feedback correction [19]. MPC has little dependence on the system model and can realize superior steady-state and dynamic per-formance [20]. There are two common MPC algorithms, namely finite control set MPC (FCS-MPC) and continuous control set MPC (CCS-MPC) [21].

For CCS-MPC, the continuous control signal is computed and then the required output is generated using a modulator. The use of a modulator allows the system to operate at a fixed switching frequency, leading to reduced harmonics in the output current [22]. In comparison, FCS-MPC simplifies the control strategy by using only one optimal voltage vector [23]. Its intuitive concept, ease of modeling, fast dynamic response, together with its ability of flexibly including various

Manuscript received November 17, 2025; revised January 8, 2026; accepted January 27, 2026. Date of publication March 30, 2026; date of current version March 11, 2026. This research was supported by the National Natural Science Foundation of China under the grant 42306260 and U23A20649, and the China Postdoctoral Science Foundation under the grant 2023M733042. (*Corresponding authors: Yinke Dou*.)

J. Lv is with the Department of Mechanical Engineering, Taiyuan University of Technology, Taiyuan 030024, China (e-mail: ljyedu@126.com).

Y. Dou and Y. Zhang are with the College of Electrical and Power Engineering, Taiyuan University of Technology, Taiyuan 030024, China (e-mail: douyinke@tyut.edu.cn; zhang.yu.edu@163.com).

Digital Object Identifier 10.24295/CPSSTPEA.2026.00002

system constraints help in meeting the requirements of modern inverter control [24]−[26]. However, FCS-MPC also presents some issues, including the substantial computational burden, model mismatch, variable switching frequency, and the difficulty in configuring the weighting coefficient. And because traditional FCS-MPC adopts single voltage vector output mode, neutral potential balance and current tracking cannot be comprehensively addressed. This results in the generation of current harmonics and neutral potential deviation. To enhance the control precision, [27]−[28] proposed a multi-voltage vector MPC algorithm to enhance system performance, through the in-order execution of multi-vectors. However, the method proposed in [27] requires the computation of vector operation time for each of the numerous small sectors, which increases the computational burden. In contrast, the algorithm proposed in [28] involves a significantly reduced number of small sectors, thereby reducing the amount of computation.

In the rolling optimization process of FCS-MPC, the traversal method is applied to assess all voltage vectors and select the optimal voltage vector through the cost function. This approach imposes a high computational requirement on the microprocessor, which is confirmed in the [29]−[32]. To reduce the calculation burden, a novel algorithm for reducing the number of the control set is proposed in [33] for five-level inverter. The method successfully reduces the vectors from 125 to 7 by taking the voltage vector of the last step and its neighboring voltage vectors as the alternative sets. However, a potential problem with this strategy is that the optimal voltage vector may not be included in the alternative set at the present moment. This may result in a compromise in the control performance of the inverter. There is a problem of neutral potential imbalance in DC capacitor of three-phase three-level T-type inverter, which is reflected in the large voltage deviation between the two capacitors. This problem will increase a lot harmonics contained in the output current of the inverter, and ultimately makes the output quality worse [34]. To address this problem, [35] proposes controlling the action time of small vectors. [36] presents a virtual voltage vector (VVV)-based method for neutral point potential balancing, which replaces medium voltage vectors (MVV) and redundant small voltage vectors (RSVV) with virtual voltage vectors to achieve neutral point potential balance. [37] introduces virtual vectors, dividing the basic vectors and virtual vectors (VV) into two candidate groups, and selects a subset from them based on the consideration of neutral point (NP) voltage balance. However, these methods do not achieve significant optimization in terms of computational complexity.

In recent years, aiming at the T-type three-level converter, academia has proposed an advanced improved FCS-MPC strategy, whose core objective is to simultaneously address the NP potential balancing problem and the computational complexity problem [38]. By optimizing the cost function and judging the large and small sectors, this strategy reduces the computational load; by adjusting the voltage vectors, it minimizes the neutral point voltage fluctuation, such that the voltage vectors that deviate from the desired voltage vector

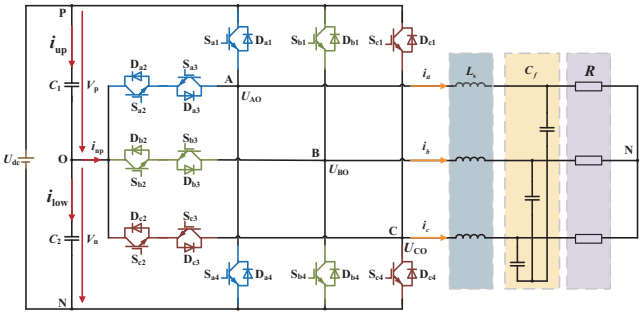

Fig. 1. Circuit diagram of the experimental platform.

reference and are not conducive to NP voltage balancing are excluded from the cost function optimization. Although it reduces the computational load and balances the neutral point potential, its sector screening based on the reference voltage introduces hidden computational overhead. These performance trade-off issues indicate that how to simultaneously balance the neutral point potential and reduce the computational load remains a key research focus in current control strategies of the same type.

To bridge the research gap identified above, this paper proposes an improved FCS-MPC approach for three-phase three-level T-type off-grid inverters. The major contributions of this research can be summarized as follows.

1) A sector optimization and vector synthesis strategy inspired by [39] is developed to improve the output current waveform and enhance the passive stabilization of neutral point voltage, which can help make the steady-state and dynamic performance better of the inverter.

2) A duration compensation mechanism of switching states is designed to promote active balance of neutral potential, and it can achieve a better effect together with the com-bination of the voltage vector.

3) Through a two-step sector determination scheme based on medium voltage vectors, the calculation burden can be greatly reduced without deterioration of system performance.

II. Traditional FCS-MPC Algorithm

A. Circuit Diagram of Inverter

Fig. 1 presents the circuit diagram of the experimental platform applied to the algorithm in this paper, where U_{dc} denotes the input voltage of the inverter, C_1 and C_2 denote the DC-side capacitosr, V_p and V_n denote the DC-side capacitor voltages, i_{up} and i_{low} denote the currents through the upper and lower DC-side capacitors. On the AC side, L_s denotes the filter inductance, C_f denotes the filter capacitance, R denotes the resistive load. In this circuit topology, bridge arms a, b, c each have four switching tubes S_{ax}, S_{bx}, S_{cx} (x =1~4), which form a combination of three switching states. The output state of bridge arm a is shown in Table I. It can be found that the switching states of S_{a1} and S_{a3}, S_{a2} and S_{a4} are complementary respectively. When S_{a1} and S_{a2} remain open, the value of output voltage U_{AO} is $U_{dc}/2$; when S_{a2} and S_{a3} remain open, the value

TABLE I
OUTPUT STATE OF BRIDGE ARM A

Switching state				Output voltage	Output state	S_{abc}
S_{a1}	S_{a2}	S_{a3}	S_{a4}	U_{AO}		
1	1	0	0	$U_{dc}/2$	P	1
0	1	1	0	0	O	0
0	0	1	1	$-U_{dc}/2$	N	-1

of output voltage U_{AO} is 0; when S_{a3} and S_{a4} remain open, the value of output voltage U_{AO} is $-U_{dc}/2$.These three output states are conventionally defined as "*P*", "*O*", and "*N*".

B. System Model

In the stationary *abc* reference frame, the three-phase output voltages $u_{xN}(x \in abc)$ can be expressed as

$$\begin{cases} u_{aN} = L_S \dfrac{di_a}{dt} + Ri_a \\ u_{bN} = L_S \dfrac{di_b}{dt} + Ri_b \\ u_{cN} = L_S \dfrac{di_c}{dt} + Ri_c \end{cases} \tag{1}$$

The stationary *abc* reference frame can be converted to the *α*-*β* reference frame by Clarke transformation, which leads to the derivation of the following expression

$$\begin{cases} u_\alpha = L_S \dfrac{di_\alpha}{dt} + Ri_\alpha \\ u_\beta = L_S \dfrac{di_\beta}{dt} + Ri_\beta \end{cases} \tag{2}$$

By applying the forward Euler method, the current derivative is obtained as

$$\begin{cases} \dfrac{di_\alpha}{dt} \approx \dfrac{i_\alpha(k+1) - i_\alpha(k)}{T_S} \\ \dfrac{di_\beta}{dt} \approx \dfrac{i_\beta(k+1) - i_\beta(k)}{T_S} \end{cases} \tag{3}$$

Substituting the result of (3) into (2), the current at the sampling instant can be predicted as

$$\begin{cases} i_\alpha(k+1) = i_\alpha(k) + \dfrac{T_S}{L_S}(u_\alpha(k) - Ri_\alpha(k)) \\ i_\beta(k+1) = i_\beta(k) + \dfrac{T_S}{L_S}(u_\beta(k) - Ri_\beta(k)) \end{cases} \tag{4}$$

As shown in Fig. 1, assume that C_1=C_2=C the currents flowing through the upper and lower capacitors can be obtained as

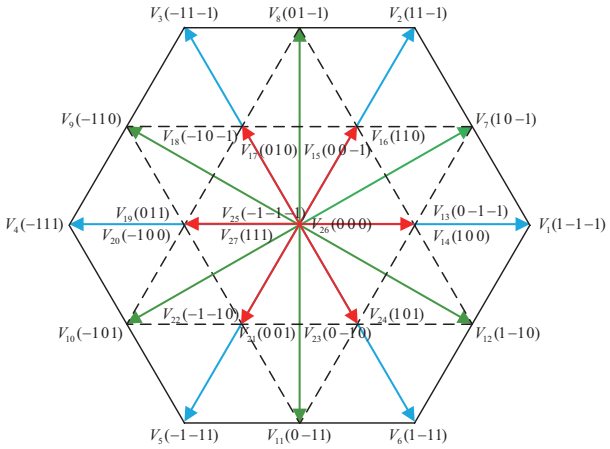

Fig. 2. Voltage vector distribution in traditional algorithm.

$$\begin{cases} i_{up} = C \dfrac{dV_p}{dt} \\ i_{low} = C \dfrac{dV_n}{dt} \end{cases} \tag{5}$$

And according to Kirchhoff's current law, the midpoint clamping current i_{np} can be expressed as

$$i_{np} = i_{up} - i_{low} \tag{6}$$

$$i_{np} = (1 - |S_A|)i_a + (1 - |S_B|)i_b + (1 - |S_C|)i_c \tag{7}$$

By using forward Euler formula, the voltage values of the upper and lower capacitors at the next time can be predicted as

$$\begin{cases} V_p(k+1) = V_p(k) + \dfrac{T_S}{C} i_{up}(k) \\ V_n(k+1) = V_n(k) + \dfrac{T_S}{C} i_{low}(k) \end{cases} \tag{8}$$

Therefore, the deviation value of the DC-link bus capacitor voltage can be obtained as

$$\begin{aligned} V_{diff} &= V_p(k+1) - V_n(k+1) \\ &= V_p(k) - V_n(k) + \frac{T_S}{C} i_{np}(k) \end{aligned} \tag{9}$$

In practice, there is a problem of NP voltage unbalance. Traditionally, this problem can be solved by incorporating the absolute value of the DC-link capacitor voltage deviation to the cost function with a weight coefficient multiplying it.

Therefore, the expression of cost function based on accurate tracking of reference current and balance of neutral point potential is shown below

$$\begin{aligned} g = (i_\alpha^*(k+1) - i_\alpha(k+1))^2 + (i_\beta^*(k+1) - \\ i_\beta(k+1))^2 + \lambda |V_{diff}| \end{aligned} \tag{10}$$

C. Traditional Control Strategy

Table I presents the switching state combination of the

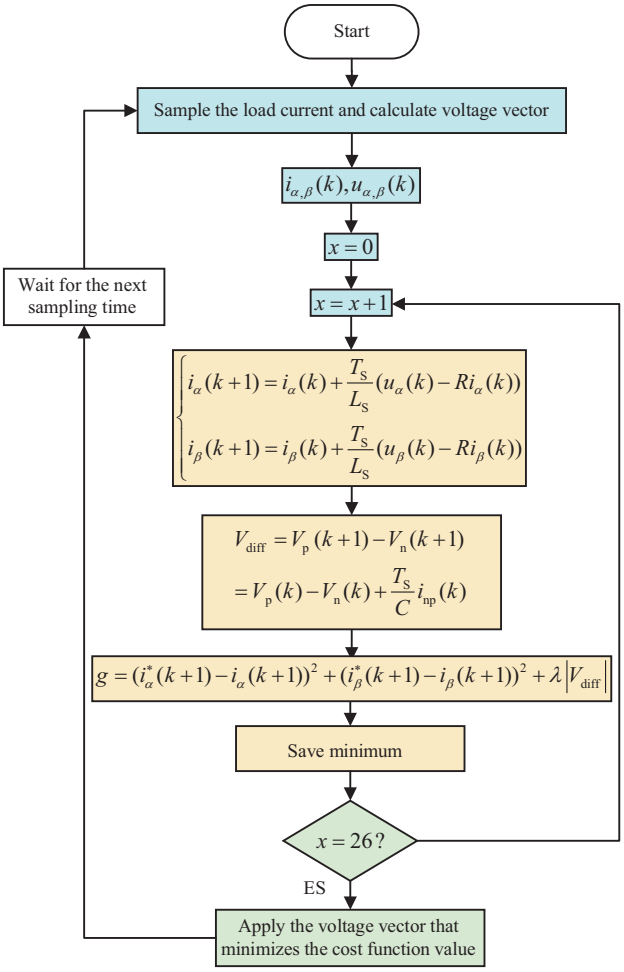

Fig. 3. Flow diagram of traditional algorithm.

three-phase three-level inverter. It is observed that a total of 27 voltage vectors will be generated, whose vector magnitudes and spatial positions are shown in Fig. 2.

In the α-β reference frame, the output voltage can be calculated by the input voltage and switching state as

$$\begin{cases} u_\alpha(k) = U_{dc}(2S_a - S_b - S_c)/6 \\ u_\beta(k) = \sqrt{3}U_{dc}(S_b - S_c)/6 \end{cases} \tag{11}$$

Fig. 3 summarizes the flowchart of the traditional FCS-MPC current control algorithm.

In the traditional FCS-MPC strategy, a single voltage vector is applied during each sampling period, which may lead to poor current tracking performance and affect the output quality. Meanwhile, although the traversal method can improve the accuracy of current tracking, it will bring a large amount of calculation and easily affect the durability of the switch tube. Since the output mode of a single voltage vector will lead to the NP voltage unbalance, it is usually necessary to use the weight coefficient in the cost function, which further increases the calculation amount and affects the comprehensive performance of the system.

In addition, due to the absence of a capacitor in current

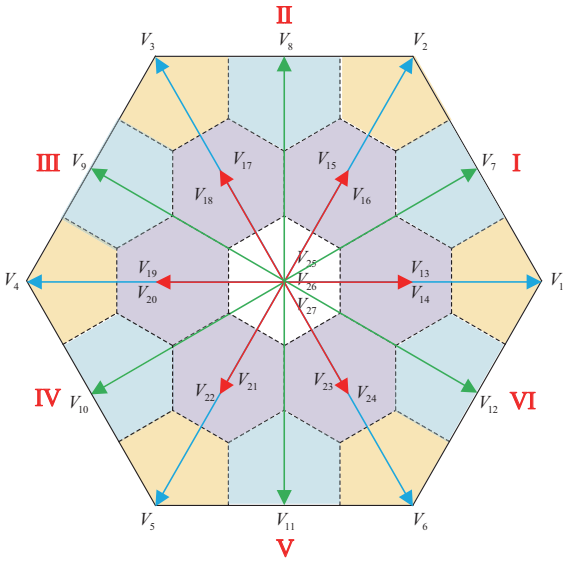

Fig. 4. Sector division and voltage vector radiation range.

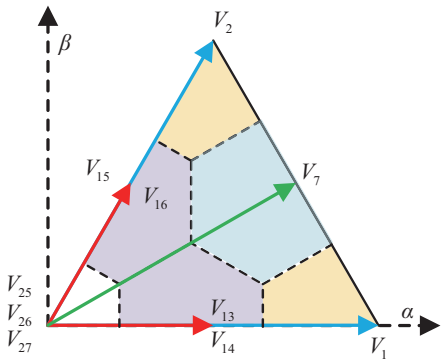

Fig. 5. Subsector division in sector I.

prediction, only inductance filtering is used in circuit topology. Therefore, when the inductance value is low, the control performance of inductance current under traditional FCS-MPC is compromised.

III. Proposed Improved FCS-MPC Algorithm

A. Sector Partitioning Optimization

This paper reconstructs the sector division according to the consideration of the effective range of the voltage vectors. In the traditional FCS-MPC algorithm, the division of subsectors tends to cause the deviation of voltage vector selection. In light of these, the improved algorithm extends the corresponding polygon area to the center of voltage vector to ensure the rationality of voltage vector selection. Fig. 4 shows the schematic diagram of the sector division and the voltage vector radiation range, while Fig. 5 shows the schematic diagram of the subsector division in sector I.

In the optimized algorithm, there are 6 sectors I~VI, with each sector being divided into 6 subsectors. For example, the subsectors are A~F in sector I. According to convention, there are 6 large voltage vectors (V_1~V_6), 6 medium voltage vectors

TABLE II
EFFECT OF MEDIUM VECTOR AND SMALL VECTOR ON THE CURRENT FLOWING THROUGH THE NEUTRAL POINT

Voltage vector	i_{np}	Voltage vector	i_{np}
V_7	i_b	V_8	i_a
V_9	i_c	V_{10}	i_b
V_{11}	i_a	V_{12}	i_c
V_{13}	i_a	V_{14}	$-i_a$
V_{15}	i_c	V_{16}	$-i_c$
V_{17}	$-i_b$	V_{18}	i_b
V_{19}	i_a	V_{20}	$-i_a$
V_{21}	$-i_c$	V_{22}	i_c
V_{23}	$-i_b$	V_{24}	i_b

TABLE III
COMBINED VECTORS V(K) IN SECTOR I

Subsector	$V(k)$
A	V_{26}
B	$\frac{1}{2}V_{13}+\frac{1}{2}V_{14}$
C	$\frac{1}{2}V_{15}+\frac{1}{2}V_{16}$
D	V_1
E	$\frac{1}{2}V_1+\frac{1}{2}V_2$
F	V_2

(V_7~V_{12}), 12 small voltage vectors (V_{13}~V_{24}) and 3 zero voltage vectors (V_{25}~V_{27}).These represent 27 basic voltage vectors.

B. Vector Synthesis and Time Compensation Mechanism

It is noted that both small and medium voltage vectors exert an influence on the neutral current of a three-phase three-level T-type inverter. Table II presents the impacts of medium and small voltage vectors on the neutral point curren.

From the table, it can be observed that both small and medium voltage vectors affect the neutral point current. However, it also shows that the corresponding small voltage vectors such as V_{15} and V_{16} can produce complementary effects on the neutral point current, that is, the neutral point current is of equal magnitude and opposite direction. Therefore, the effects of the small voltage vectors on the current flowing through the neutral point can be offset by the synthesis of the corresponding voltage vectors. At the same time, the influences of the medium voltage vectors on the neutral point current can be solved by the synthesis of large voltage vectors. In this way, the neutral potential deviation caused by the neutral point current can be eliminated theoretically, so as to achieve a simple passive balancing strategy.

Take sector I as an example, the combination path of the voltage vectors is presented in Table III.

Voltage vector synthesis can effectively mitigate the neutral point potential deviation caused by the selection of the target

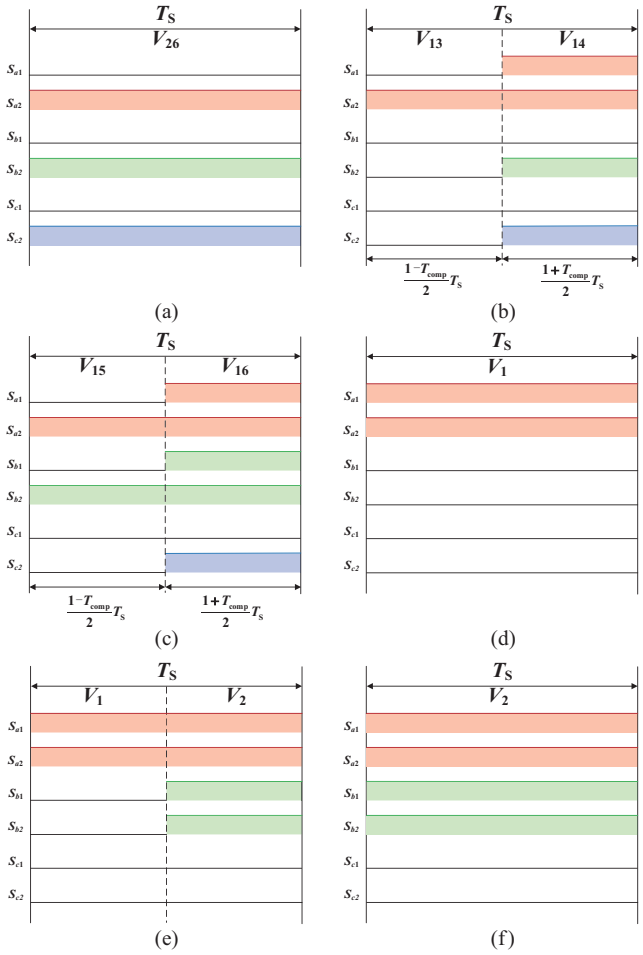

Fig. 6. Schematic diagram of switching sequence and execution time of each voltage vector in sector I. (a) Subsector A, (b) Subsector B, (c) Subsector C, (d) Subsector D, (e) Subsector E, (f) Subsector F.

voltage vector. However, the simple passive balancing strategy cannot achieve complete effectiveness due to practical errors. Thus, an action time compensation mechanism about the voltage vector is introduced here. The bus capacitor voltage can be dynamically regulated by adjusting the action time of different voltage vectors in one cycle. According to the ratio of the DC bus capacitance voltage deviation to the DC bus voltage, the time compensation factor T_{comp} can be defined as

$$T_{comp}=\frac{V_P-V_N}{V_P+V_N} \tag{12}$$

Since the voltage difference between the two capacitors mainly arises from the influence of small voltage vectors, it is only necessary to adjust the related synthesis voltage vector process. For example in sector I, the operation times of V_{13} and V_{14} in subsector B need to be adjusted, while the operation times of V_{15} and V_{16} in subsector C need to be adjusted, as illustrated in Fig. 6.

Through the voltage vector synthesis and the corresponding action time compensation mechanism, the neutral potential balance can be realized without the weight coefficient in the traditional cost function. The optimized cost function can be obtained as

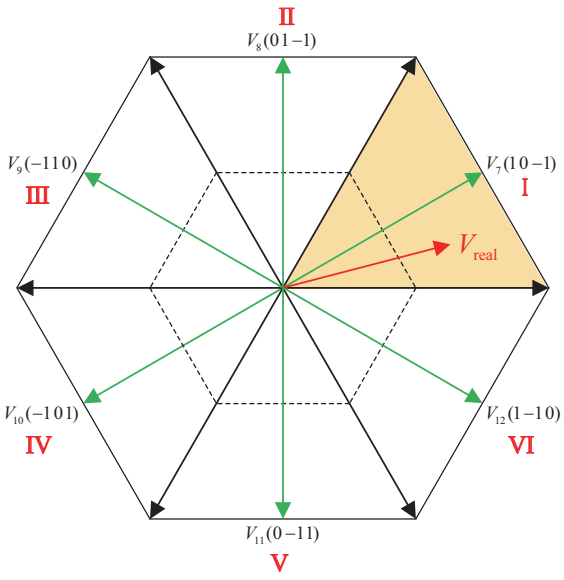

Fig. 7. Two-step sector determination diagram.

$$g = (i_\alpha^*(k+1) - i_\alpha(k+1))^2 + (i_\beta^*(k+1) - i_\beta(k+1))^2 \quad (13)$$

However, this algorithm leads to repeated calculations of many voltage vectors, greatly increasing the amount of computation.

C. Two-Step Sector Determination

Fig. 7 shows the two-step sector determination diagram.

D. Algorithm Flow of The Proposed FCS-MPC

Fig. 8 shows the flow chart of the proposed improved algorithm. The process starts with initial sampling and calculation, then executes the first-step sector selection according to the current prediction formula, thereby confining the target voltage vector within the corresponding sector range Its control block diagram is presented in Fig. 9. The target voltage vector is subsequently chosen in the corresponding sector, and the current prediction formula is applied again to identify the reference voltage vector that minimizes the cost function. Finally, the inverter adopts the switching state corresponding to the selected reference voltage vector. The cost function is essential in the entire process, which not only affects the accuracy of sector selection in the secondary judgment, but also determines the final current tracking performance.

IV. Experimental Results

To prove the feasibility and effectiveness of the above optimization algorithm, an experimental platform was constructed using a three-phase three-level T-type off-grid inverter. It was implemented using Digital Signal Processor (DSP) TMS320F28377D. The experiment parameters are presented in Table IV.

In this section, a comparison is conducted among the traditional FCS-MPC algorithm with weight coefficients,

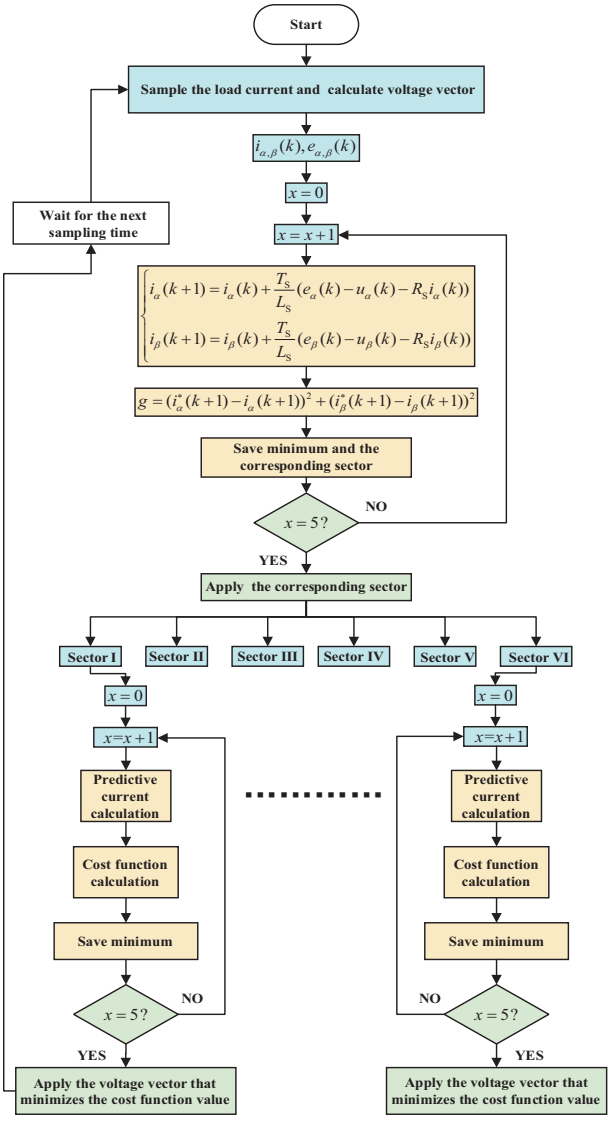

Fig. 8. Flow diagram of proposed algorithm.

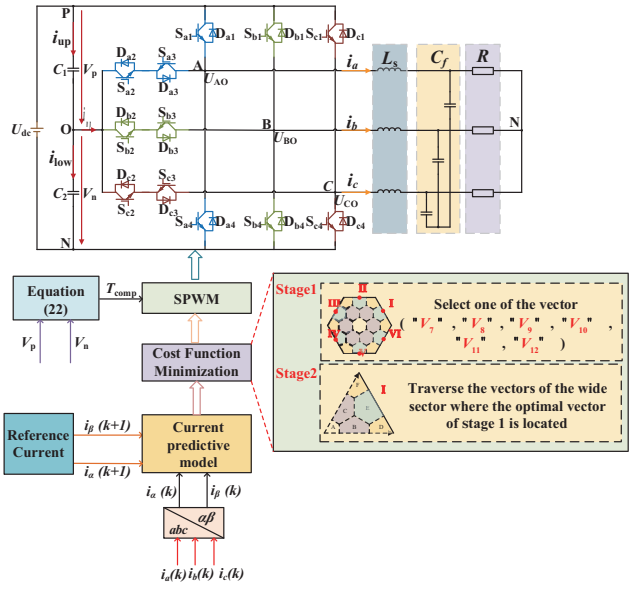

Fig. 9. Control block diagram of the proposed algorithm.

TABLE IV
EXPERIMENT PLATFORM PARAMETERS

Parameters	Terminology interpretation	Numerical value
U_{dc}	Bus voltage	200 V
R	Loads	10 Ω
i_{ref}	Reference current	5.5~3 A
C_1, C_2	DC-link capacitors	100 μF
L_S	Filter inductance	4 mH
C_f	Filter capacitor	5 μF
f_S	Sampling frequency	16 kHz

TABLE V
CODE OPERATION TIME

Algorithm	Code operation time	
	Counting points	Actual time
Traditional FCS-MPC	6276	31.38 μs
Improved FCS-MPC	3018	15.09 us
Proposed FCS-MPC	1733	8.67 μs

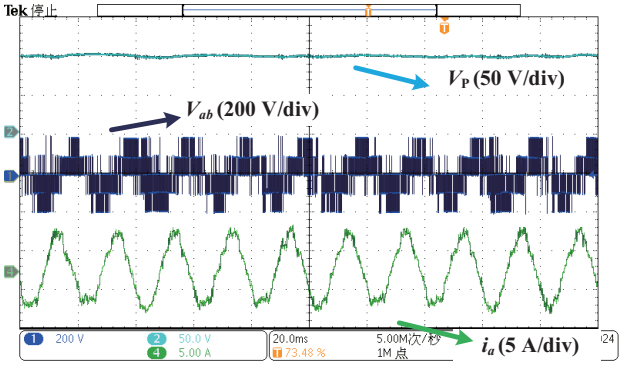

Fig. 10. Steady-state experimental results with the traditional strategy when i_{ref} is 5.5 A.

the improved FCS-MPC algorithm proposed in [38] and the optimized FCS-MPC algorithm without weight coefficients.

A. Algorithm Execution Time

In order to verify that the optimization algorithm can effectively reduce the computational complexity, the execution time of the three algorithms is calculated by the clock function of the code composer studio in the experiment to evaluate. The specific results are presented in Table V: the actual operation time of the optimized algorithm is 8.67 μs, which is only 27.63% of that of the traditional algorithm and 57.45% of that of the improved algorithm. This verifies the effectiveness of the two-step sector determination strategy.

B. Steady-State Performance Evaluation

In order to make the traditional FCS-MPC strategy achieve

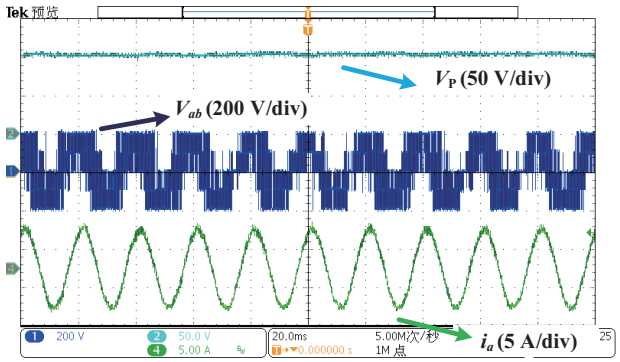

Fig. 11. Steady-state experimental results with the improved strategy when i_{ref} is 5.5 A.

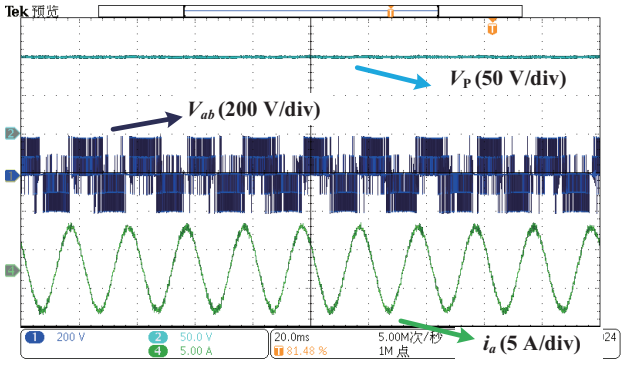

Fig. 12. Steady-state experimental results with the proposed strategy when i_{ref} is 5.5 A.

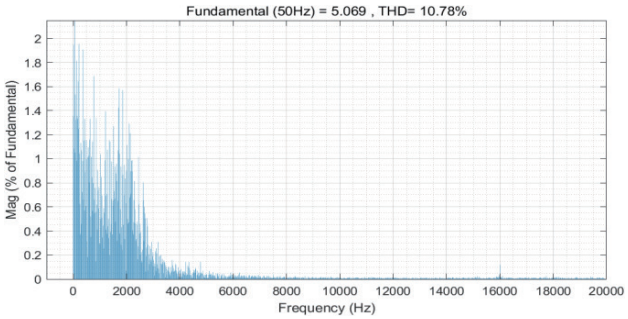

Fig. 13. Steady-state total harmonic distortion of current with the traditional strategy when i_{ref} is 5.5 A.

a more effective NP balance, the weight coefficient is set to 0.5 to facilitate the following comparison experiments.

Figs. 10, 11, and 12 respectively show the inverter output voltage V_{ab}, output current i_a and DC bus upper capacitor voltage V_P under the three strategies. Figs. 13, 14 and 15 show the total harmonic distortion of current i_a under these three strategies.

A comparison between Figs. 10, 11, and 12 reveals that both the traditional algorithm and the improved algorithm fail to achieve good current tracking performance under the condition of a low inductance value, although it can achieve good current tracking effect after sector optimization and vector combination. In addition, when i_{ref} is 5.5 A, the total harmonic distortion of the output current is 10.78% for the traditional algorithm, 8.21% for the improved MPC algorithm, and 5.06% for the proposed

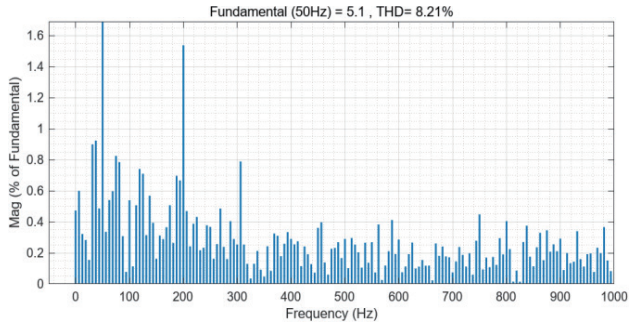

Fig. 14. Steady-state total harmonic distortion of current with the improved strategy when i_{ref} is 5.5 A.

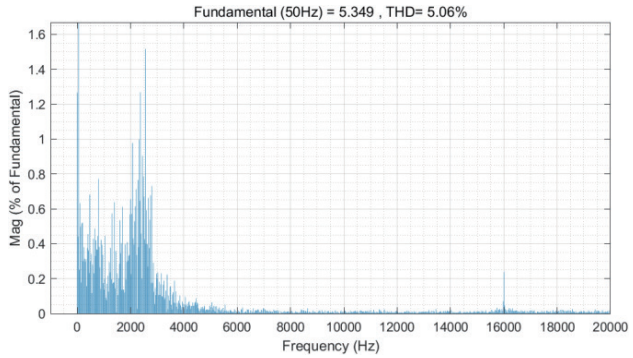

Fig. 15. Steady-state total harmonic distortion of current with the proposed strategy when i_{ref} is 5.5 A.

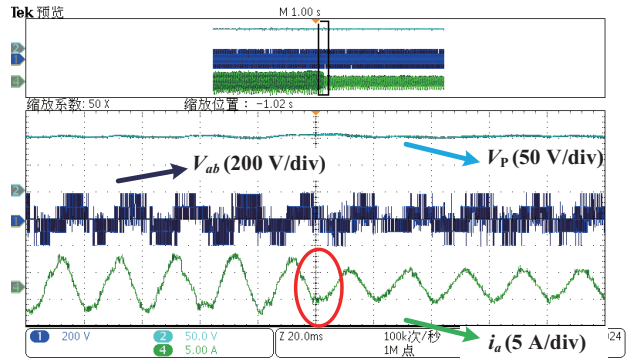

Fig. 16. Dynamic experimental results with the traditional strategy when i_{ref} changes from 5.5 A to 3 A.

algorithm. This is mainly because the proposed algorithm is more accurate in the voltage vector selection process. And it should be noted that the high-order harmonics are mainly concentrated near the sampling frequency (16 kHz). To sum up, it can be proved that the proposed algorithm has significant advantages in improving current output quality and ensuring current steady-state performance.

C. Dynamic Performance Evaluation

Figs. 16, 17, and 18 illustrate, respectively, the response characteristics of the inverter output voltage, output current and DC bus capacitor voltage when the current is decreased from 5.5 A to 3 A under the traditional algorithm, improved algorithm and proposed algorithm.

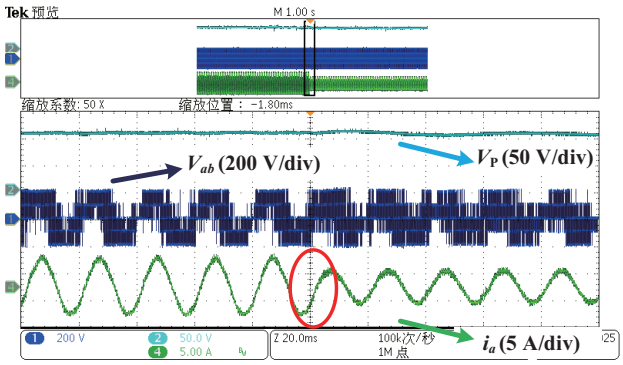

Fig. 17. Dynamic experimental results with the improved strategy when i_{ref} changes from 5.5 A to 3 A.

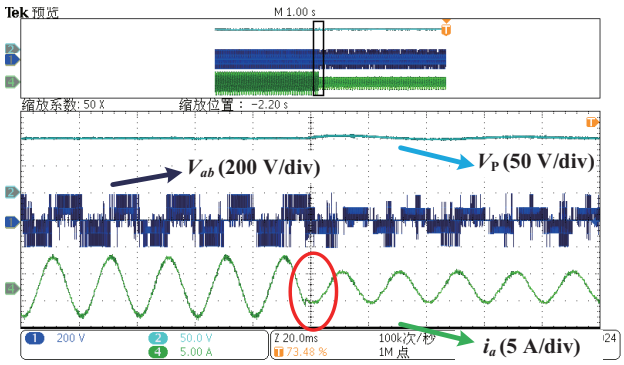

Fig. 18. Dynamic experimental results with the proposed strategy when i_{ref} changes from 5.5 A to 3 A.

As can be seen from the figures, all three algorithms are able to complete current tracking within approximately 2.5 ms under the condition of current abrupt change, which indicates that they all achieve excellent transient response performance. However, the proposed algorithm exhibits significantly better output current quality both before and after the reference current mutation.

D. Neutral Potential Balance Analysis

Although the traditional algorithm can also achieve neutral potential balance by using the weight coefficient in the cost function, this approach significantly increases the computational load and results in a biased selection of voltage vectors. Although the improved algorithm does not require the introduction of weight coefficients, it incurs hidden computational overhead due to the sector selection based on the reference voltage. On the other hand, the proposed algorithm is able to address this issue while the neutral potential balance can be maintained. Figs. 19, 20, and 21 show the steady-state fluctuation of the DC bus capacitor voltage under the three algorithms when i_{ref} is 5.5 A. Meanwhile, Figs. 22, 23, and 24 show the dynamic fluctuation of the DC bus capacitor voltage under the three algorithms when i_{ref} decreases from 5.5 A to 3 A. From the comparison of steady-state results, it can be observed that the fluctuation amplitude of the neutral point potential is

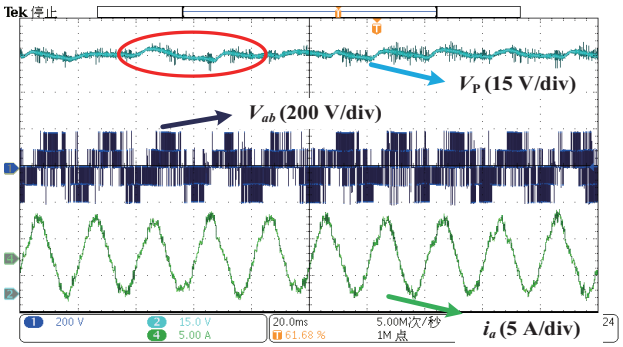

Fig. 19. Steady-state upper capacitor voltage V_P fluctuation with the traditional strategy when i_{ref} is 5.5 A.

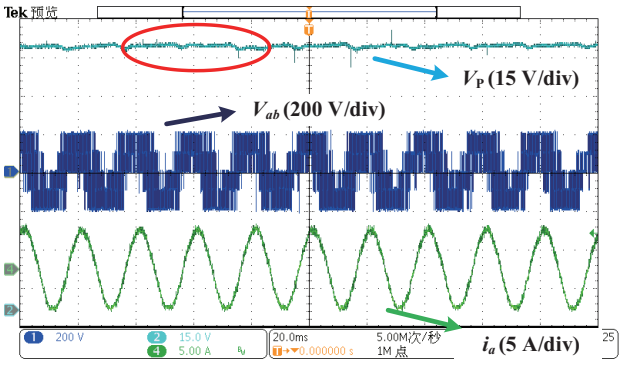

Fig. 20. Steady-state upper capacitor voltage V_P fluctuation with the improved strategy when i_{ref} is 5.5 A.

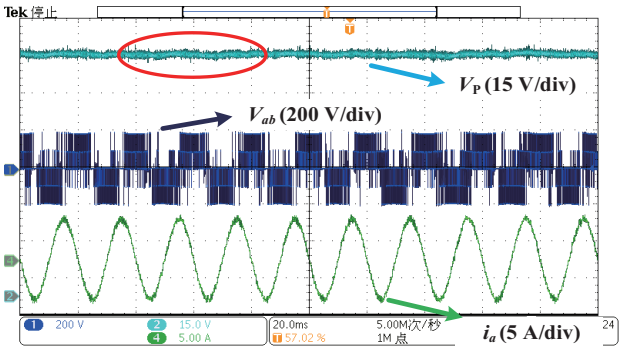

Fig. 21. Steady-state upper capacitor voltage V_P fluctuation with the proposed strategy when i_{ref} is 5.5 A.

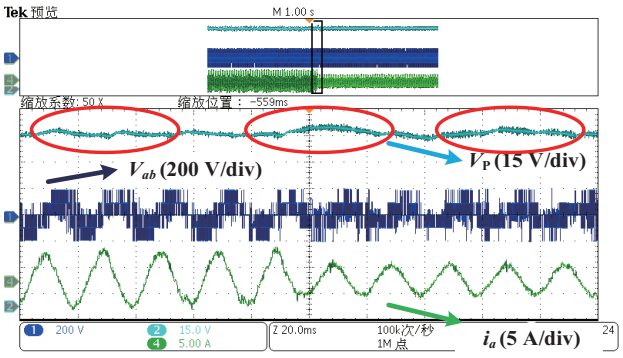

Fig. 22. Dynamic upper capacitor voltage V_P fluctuation with the traditional strategy when i_{ref} changes from 5.5 A to 3 A.

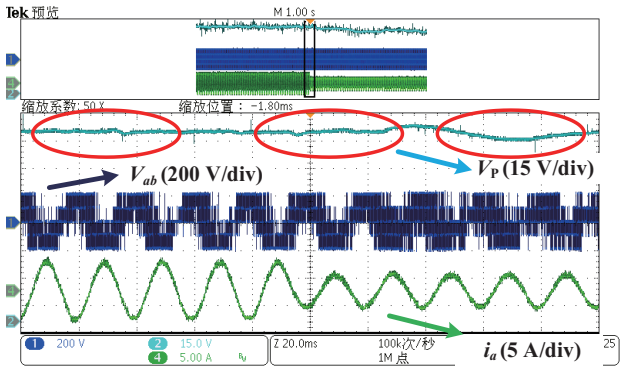

Fig. 23. Dynamic upper capacitor voltage V_P fluctuation with the improved strategy when i_{ref} changes from 5.5 A to 3 A.

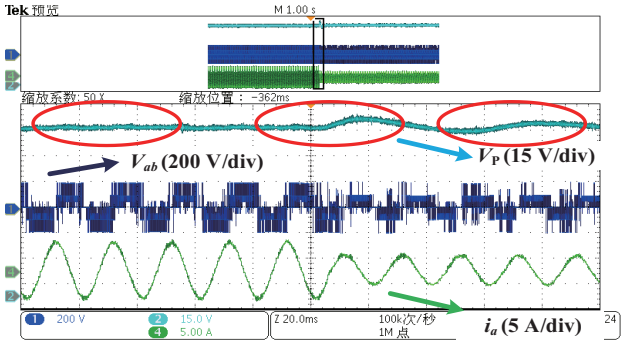

Fig. 24. Dynamic upper capacitor voltage V_P fluctuation with the proposed strategy when i_{ref} changes from 5.5 A to 3 A.

approximately 4 V under the traditional algorithm and around 3 V under the improved algorithm, while the fluctuation amplitude of the neutral point potential is generally maintained at 3 V for the proposed algorithm, thus yielding a more stable waveform. From the dynamic comparison graphs, it can be found that under both algorithms, although a transient fluctuation occurs in the neutral point potential when i_{ref} changes, the potential can quickly recover to the rated value (100 V).

In summary, the proposed algorithm can further achieve lower voltage fluctuation under the premise of ensuring the balance of the neutral point potential. This means that the voltage vector synthesis and time compensation mechanism are effective.

E. System Stability Analysis

In practice, interference factors such as model incompatibility and parameter errors should be considered. Thus, robustness analysis is a key step to verify system stability. In this test, the inductance L_s is reduced from 4 mH to 3 mH in the proposed control algorithm. A comparison between Fig. 12 and Fig. 25 reveals that after reducing the inductance parameter by 1 mH (25%), the inverter output voltage V_{ab}, output current i_a and DC bus upper capacitor voltage V_P are not significantly affected. A comparison between Fig. 15 and Fig. 26 illustrates that the total harmonic distortion of the output current is only increased by 0.29% when the inductance parameter is deviated. These results demonstrate that the proposed algorithm maintains stable

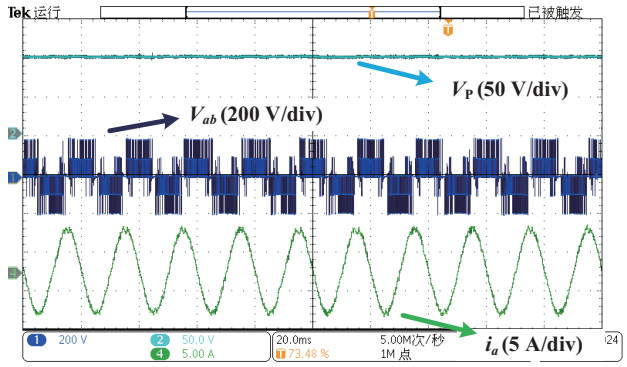

Fig. 25. Steady-state experimental results with L_S reduced to 3 mH under the proposed strategy when i_{ref} is 5.5 A.

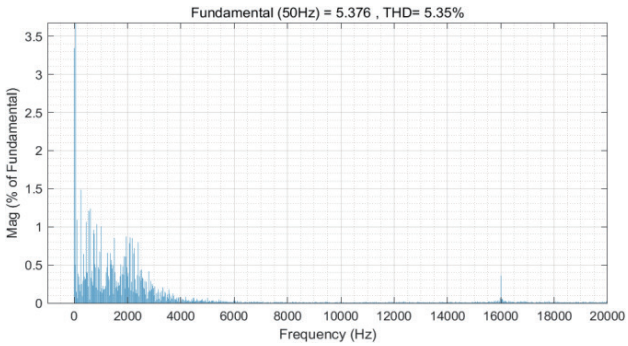

Fig. 26. Steady-state total harmonic distortion of current with L_S reduced to 3 mH under the proposed strategy when i_{ref} is 5.5 A.

performance despite changes in system parameters.

V. Conclusion

An optimized FCS-MPC algorithm for three-phase three-level T-type off-grid inverter is proposed in this paper, with a marked reduction in current ripple by means of subsector redivision and voltage vector synthesis. To enhance the balance of the neutral point potential, the time compensation mechanism is introduced with the voltage vector synthesis being used to complement the passive balance. On this basis, a two-step sector determination strategy is proposed to solve the problem of excessive computation. In this paper, the optimization algorithm is analyzed comprehensively from a theoretical standpoint and proved by rigorous experiments.

Based on these theoretical analysis and preliminary simulation research, a number of experiments are conducted in this study. The experimental results show that compared with the traditional algorithm, the computational complexity of the proposed optimized algorithm is only 27.63% of that of the traditional algorithm and 57.45% of that of the improved algorithm. All three algorithms can achieve excellent dynamic performance, yet the proposed optimized algorithm exhibits superior steady-state performance, with the total harmonic distortion (THD) of its output current being only 46.8% of that of the traditional algorithm and 61.6% of that of the improved algorithm. All three algorithms are capable of realizing neutral point potential balance, while the proposed optimized algorithm can minimize the voltage fluctuation amplitude. It can also be seen from the stability experiment that although the inductance parameters in the algorithm are changed, the total harmonic distortion does not change significantly. That is to say, the stability of the system can be guaranteed. These conclusions all prove the effectiveness of the optimization algorithm.

References

[1] B. Kroposki, B. Johnson, Y. Zhang, V. Gevorgian, P. Denholm, B.-M. Hodge, and B. Hannegan, "Achieving a 100% renewable grid: operating electric power systems with extremely high levels of variable renewable energy," in *IEEE Power and Energy Magazine*, vol. 15, no. 2, pp. 61–73, Mar.-Apr. 2017.

[2] S. Xu, Y. Guo, and W. Su, "A proof-of-concept demonstration for the transportation electrification education," in *2014 IEEE Conference and Expo Transportation Electrification Asia-Pacific (ITEC Asia-Pacific)*, Beijing, 2014, pp. 1–5.

[3] K. Chaiyaphun, P. Santiprapan, C. Panpean, and K. Areerak, "Power angle control of a unified power quality conditioner in railway electrification system," in *2023 IEEE Transportation Electrification Conference and Expo, Asia-Pacific (ITEC Asia-Pacific)*, Chiang Mai, Thailand, 2023, pp. 1–8.

[4] X. Wang, Y. Han, L. Li, J. Wang, W. Chen, and W. Shen, "CVaR quantitative uncertainty-based optimal dispatch for flexible traction power supply system," in *IEEE Transactions on Transportation Electrification*, vol. 10, no. 1, pp. 1900–1910, Mar. 2024.

[5] J. Pan, Y. Yang, J. Li, F. Wang, Y. Abdullah, and L. Xu, "Control of high-performance drive feeding by four-level hybrid clamped converter for transportation electrification," in *IEEE Transactions on Transportation Electrification*, vol. 6, no. 2, pp. 568–577, Jun. 2020.

[6] D. Schwanz, F. Möller, S. K. Rönnberg, J. Meyer, and M. H. J. Bollen, "Stochastic assessment of voltage unbalance due to single-phase-connected solar power," in *IEEE Transactions on Power Delivery*, vol. 32, no. 2, pp. 852–861, Apr. 2017.

[7] V. F. Pires, A. Cordeiro, D. Foito, and J. F. Silva, "A STATCOM based on a three-phase, triple inverter modular topology for multilevel operation," in *IEEE Transactions on Power Delivery*, vol. 34, no. 5, pp. 1988–1997, Oct. 2019.

[8] S. D. Ratrey, A. Hota, V. Sonti, and S. Jain, "A new three-phase three-level inverter obtained from two-level inverter by considering the effect of device junction capacitance across the switch," in *2023 IEEE 3rd International Conference on Sustainable Energy and Future Electric Transportation (SEFET)*, Bhubaneswar, India, 2023, pp. 1–5.

[9] N. Altin, I. Sefa, H. Komurcugil, and S. Ozdemir, "Three-phase three-level T-type grid-connected inverter with reduced number of switches," in *2018 6th International Istanbul Smart Grids and Cities Congress and Fair (ICSG)*, Istanbul, Turkey, 2018, pp. 58–62.

[10] N. Soualhi, A. Makouf, N. Nait-Said, and S. Hamada, "Comparison between a Two-Level and Three-Level Inverter fed Induction Motor including Losses and Efficiency," in *2020 4th International Conference on Advanced Systems and Emergent Technologies (IC_ASET)*, Hammamet, Tunisia, 2020, pp. 89–94.

[11] A. Palanisamy, A. Mahajaran, S. Liese, Y. Siwakoti, T. Long, Omid Forati Kashani, and F. Blaabjerg, "A new three-level three-phase Boost PWM inverter for PV applications," in *2018 IEEE Energy Conversion Congress and Exposition (ECCE)*, Portland, OR, USA, 2018, pp. 7191–7196.

[12] Q. -B. Nguyen, P. C. Dung, H. -C. Vu, T. N. Dinh, and Q. -H. Tran, "A modulated model predictive control for Three-Phase three-level T-type inverter," in *2022 11th International Conference on Control, Automation and Information Sciences (ICCAIS)*, Hanoi, Vietnam, 2022, pp. 190–195.

[13] H. -S. Kim, Y. -C. Kwon, S. -J. Chee, and S. -K. Sul, "Analysis and compensation of inverter nonlinearity for three-level T-type inverters," in *IEEE Transactions on Power Electronics*, vol. 32, no. 6, pp. 4970–4980, Jun. 2017.

[14] M. Lak, T. -L. Wu, and T. -L. Lee, "A hybrid method for three-level T-type inverters to eliminate neutral point voltage ripple and control DC-link capacitors' in Voltage for Separate MPPT," in *IEEE Access*, vol. 9, pp. 148650–148664, 2021.

[15] N. B. A and P. Agarwal, "Nearest and non-nearest three vector modulations of NPCI using two-level space vector diagram—a novel

approach," in *IEEE Transactions on Industry Applications*, vol. 54, no. 3, pp. 2400–2415, May-Jun. 2018.
[16] S. Bhowmik, P. K. Gayen, and A. Mitra, "Performance comparison between PI based control and model predictive control of voltage source inverter under load variations," in *2022 IEEE International Conference of Electron Devices Society Kolkata Chapter (EDKCON)*, Kolkata, India, 2022, pp. 344–348.
[17] Y. Zhang, Z. Wang, J. Jiao, and J. Liu, "Grid-voltage sensorless model predictive control of three-phase PWM rectifier under unbalanced and distorted grid voltages," in *IEEE Transactions on Power Electronics*, vol. 35, no. 8, pp. 8663–8672, Aug. 2020.
[18] D. Chen, J. Zhang, and Z. Qian, "An improved repetitive control scheme for grid-connected inverter with frequency-adaptive capability," in *IEEE Transactions on Industrial Electronics*, vol. 60, no. 2, pp. 814–823, Feb. 2013.
[19] Y. Yang, H. Wen, M. Fan, M. Xie, R. Chen, and Y. Wang, "A constant switching frequency model predictive control without weighting factors for T-type single-phase three-level inverters," in *IEEE Transactions on Industrial Electronics*, vol. 66, no. 7, pp. 5153–5164, Jul. 2019.
[20] R. Errouissi, S. M. Muyeen, A. Al-Durra, and S. Leng, "Experimental validation of a robust continuous nonlinear model predictive control based grid-interlinked photovoltaic inverter," in *IEEE Transactions on Industrial Electronics*, vol. 63, no. 7, pp. 4495–4505, Jul. 2016.
[21] Y. Yang, Y. Xiao, M. Fan, K. Wang, X. Zhang, J. Hu, G. Fang, W. Zeng, S. Vazquez, and J. Rodriguez, "A novel continuous control set model predictive control for LC-filtered three-phase four-wire three-level voltage-source inverter," in *IEEE Transactions on Power Electronics*, vol. 38, no. 4, pp. 4572–4584, Apr. 2023.
[22] F. Toso, A. Favato, R. Torchio, P. Alotto, and S. Bolognani, "Continuous control set model predictive current control of a microgrid-connected PWM inverter," in *IEEE Transactions on Power Systems*, vol. 36, no. 1, pp. 415–425, Jan. 2021.
[23] S. Vazquez, J. Rodriguez, M. Rivera, L. G. Franquelo, and M. Norambuena, "Model predictive control for power converters and drives: advances and trends," in *IEEE Transactions on Industrial Electronics*, vol. 64, no. 2, pp. 935–947, Feb. 2017.
[24] P. Falkowski and A. Sikorski, "Finite control set model predictive control for grid-connected AC-DC converters with LCL filter," in *IEEE Transactions on Industrial Electronics*, vol. 65, no. 4, pp. 2844–2852, Apr. 2018.
[25] X. Li, H. Zhang, M. B. Shadmand, and R. S. Balog, "Model predictive control of a voltage-source inverter with seamless transition between islanded and grid-connected operations," in *IEEE Transactions on Industrial Electronics*, vol. 64, no. 10, pp. 7906–7918, Oct. 2017.
[26] S. Sajadian and R. Ahmadi, "Model predictive control of dual-mode operations Z-source inverter: islanded and grid-connected," in *IEEE Transactions on Power Electronics*, vol. 33, no. 5, pp. 4488–4497, May 2018.
[27] F. Donoso, A. Mora, R. Cárdenas, A. Angulo, D. Sáez, and M. Rivera, "Finite-set model-predictive control strategies for a 3L-NPC inverter operating with fixed switching frequency," in *IEEE Transactions on Industrial Electronics*, vol. 65, no. 5, pp. 3954–3965, May 2018.
[28] A. Mora, R. Cárdenas-Dobson, R. P. Aguilera, A. Angulo, F. Donoso, and J. Rodriguez, "Computationally efficient cascaded optimal switching sequence MPC for grid-connected three-level NPC converters," in *IEEE Transactions on Power Electronics*, vol. 34, no. 12, pp. 12464–12475, Dec. 2019.
[29] Y. Zhang and W. Xie, "Low complexity model predictive control—single vector-based approach," in *IEEE Transactions on Power Electronics*, vol. 29, no. 10, pp. 5532–5541, Oct. 2014.
[30] Y. Zhang, W. Xie, Z. Li, and Y. Zhang, "Low-complexity model predictive power control: double-vector-based approach," in *IEEE Transactions on Industrial Electronics*, vol. 61, no. 11, pp. 5871–5880, Nov. 2014.
[31] C. Xia, T. Liu, T. Shi, and Z. Song, "A simplified finite-control-set model-predictive control for power converters," in *IEEE Transactions on Industrial Informatics*, vol. 10, no. 2, pp. 991–1002, May 2014.
[32] C. -K. Lin, T. -H. Liu, J. -t. Yu, L. -C. Fu, and C. -F. Hsiao, "Model-free predictive current control for interior permanent-magnet synchronous motor drives based on current difference detection technique," in IEEE Transactions on Industrial Electronics, vol. 61, no. 2, pp. 667–681, Feb. 2014.
[33] M. A. Perez, P. Cortes, and J. Rodriguez, "Predictive control algorithm technique for multilevel asymmetric cascaded H-bridge inverters," in *IEEE Transactions on Industrial Electronics*, vol. 55, no. 12, pp. 4354–4361, Dec. 2008.
[34] L. Dong, Z. Zang, Y. Ming, R. Zhao, W. Ma, and H. Hu, "Research on the coordination suppression strategy of neutral point potential and common mode voltage for NPC three-level inverter" in *Symmetry*, vol. 15, no. 1, pp. 35, Jan. 2023.
[35] N. Li, Y. Wang, R. Niu, W. Guo, W. Lei, and Z. Wang, "A novel neutral point voltage automatic balancing carrier-based modulation strategy of three-level NPC converter," in *2014 International Power Electronics Conference (IPEC-Hiroshima 2014 - ECCE ASIA)*, Hiroshima, Japan, 2014, pp. 475–479.
[36] S. Lotfollahzadegan, S. A. Davari, C. Garcia, and J. Rodriguez, "Capacitors voltage balancing in neutral-point clamped inverter using simplified finite set model predictive control and virtual voltage vectors," in *2020 11th Power Electronics, Drive Systems, and Technologies Conference (PEDSTC)*, Tehran, Iran, 2020, pp. 1–6.
[37] N. Jin, H. Li, Z. Xu, and L. Guo, "A model predictive control strategy with virtual vectors visualization analysis for NPC converter without weighting factor," in *2025 IEEE International Conference on Predictive Control of Electrical Drives and Power Electronics (PRECEDE)*, Nanjing, China, 2025, pp. 1–5.
[38] Y. Yang, H. Wen, M. Fan, M. Xie, and R. Chen, "Fast finite-switching-state model predictive control method without weighting factors for T-type three-level three-phase inverters," in *IEEE Transactions on Industrial Informatics*, vol. 15, no. 3, pp. 1298–1310, Mar. 2019.
[39] S. Yan, Y. Cui, C. Li, X. Gao, and Y. Cai, "An improved FCS-MPC based on novel sector optimization and capacitor charge balance algorithm for T-type 3P-3L converters," in *IEEE Transactions on Power Electronics*, vol. 38, no. 4, pp. 4559–4571, Apr. 2023.

Jinyu Lv was born in 1979. He was admitted to Taiyuan University of Technology to major in Electrical Engineering and Automation in 1997, and later received the M.E. degree in Engineering in the field of Electrical Engineering. He obtained the Ph.D. degree in Mechanical Engineering from Taiyuan University of Technology, with his doctoral research focusing on low-wind-speed wind power generation systems and inverter research, as well as distributed energy storage systems and bidirectional inverter research.

Yinke Dou was born in Fengxiang, Shaanxi, China, in 1973. He received the B.E. degree in Engineering, the M.E. degree in Monitoring Technology and Automation, and the Ph.D. degree in Engineering in Circuits and Systems from the Taiyuan University of Technology, in 1997, 2005, and July 2010, respectively. He is currently a Professor and a Ph.D. supervisor.

Yu Zhang was born in 1987. He obtained the M.E. degree in Electrical Engineering from Dalian University of Technology in 2012 and is currently a Ph.D. candidate in electrical engineering at Taiyuan University of Technology. He is currently the director of the Teaching Experiment Center of the Department of Automation at Taiyuan University of Technology. He became a senior engineer in December 2019. In 2022, he joined the Shanxi Energy Internet Research Institute as the head of research and development (administrative leader) of the Polar and Extreme Environment Energy Equipment Design and Manufacturing Team.